Journal of Magnetic Resonance **150,** 49–56 (2001)
doi:10.1006/jmre.2001.2316, available online at http://www.idealibrary.com on IDEAL®

Macroscopic Background Gradient and Radiation Damping Effects on High-Field PGSE NMR Diffusion Measurements

William S. Price,* Peter Stilbs,* Bengt Jönsson,† and Olle Söderman†

*Physical Chemistry, Royal Institute of Technology, SE-100 44 Stockholm, Sweden; and †Department of Physical Chemistry 1, Center for Chemistry and Chemical Engineering, Lund University, P.O. Box 124, S-221 00 Lund, Sweden

Received October 23, 2000; revised January 30, 2001; published online April 17, 2001

The effects of macroscopic background gradients due to susceptibility differences at the sample interfaces and of radiation damping on pulsed-gradient spin-echo (PGSE) experiments are examined. Both phenomena can lead to the seemingly strange effect of the echo signal growing as the gradient strength increases at low applied gradient strengths. For a freely diffusing species, background gradients manifest themselves as slight concave or convex inflections in the linearized PGSE attenuation curve, depending on the polarity of the applied gradient. The various means of overcoming macroscopic background gradient problems, including bipolar gradients, and their efficacy are examined experimentally and discussed. The effects of radiation damping can also result in the attenuation curve being nonlinear but, different from the effect of background gradients, the nonlinearity does not change with the polarity of the applied gradient. The vulnerability of the stimulated echo-based PGSE sequence and variations of Hahn-based PGSE sequences is investigated. Both background gradients and radiation damping have serious implications for accurate diffusion measurement determination.

Key Words: **background gradients; bipolar gradients; calibration; diffusion; PGSE; radiation damping.**

INTRODUCTION

Pulsed-gradient spin-echo (PGSE) NMR is becoming the method of choice for measuring translational diffusion (also known as self-diffusion or intradiffusion) coefficients (D) (e.g., see Refs. (*1–3*)). The generation of eddy currents and the requirement for a constant (commonly, although erroneously, referred to as "linear") gradient over the sample volume are well-known problems and both of these effects can reduce the accuracy of the diffusion coefficients determined. Care must also be taken to avoid convection (*4*) and mismatched gradient pulses (*5*). Nevertheless, even after accounting for these deleterious factors, the error in a PGSE measurement is generally not much less than 1% (*6*).

Two other complications that seriously reduce the accuracy of PGSE measurements but that have received less attention are (*1*) background gradients due to the magnetic susceptibility differences at sample interfaces (i.e., the "meniscus effect") and (*2*) radiation damping. Problems due to background gradients are well known (e.g., (*7*) and references therein) but previous discussion has been limited to microscopic magnetic inhomogeneities in samples (e.g., biological systems, colloidal suspensions, metal hydrides, and porous systems) (*8–14*), although the artifacts caused by macroscopic susceptibility gradients are well known in NMR microscopy (*15–17*) and in other areas of NMR spectroscopy (*18–21*). Radiation damping, and the associated problem of the dipolar field, is a well-known source of artifacts in NMR and is known to lead to phenomena such as multiple echoes (e.g., (*22–26*)). However, the effects of radiation damping on PGSE measurements have not previously been investigated in detail. Importantly, the severity of both of these complications increases with the static magnetic field strength, $\mathbf{B}_0$.

Here we investigate the problems that result from macroscopic background gradients and radiation damping and how these problems can be alleviated, thereby increasing the accuracy of the diffusion coefficients determined. Some simple modifications to pulse sequences are proposed.

THEORY

Macroscopic Gradients

Assuming that the gradient pulses of duration δ and magnitude g are applied in the presence of a constant background gradient g_0, the attenuation (i.e., the echo signal S, divided by the signal acquired with $g = 0$, S_0) due to diffusion in the Hahn spin-echo-based PGSE sequence (Fig. 1A) is (*1*)

$$E(g, g_0) = \frac{S}{S_0} = \exp\left(-\gamma^2 \left[\underbrace{g^2 D\delta^2(\Delta - \delta/3)}_{\mathbf{g}\text{ term}} + \underbrace{\mathbf{g}\cdot\mathbf{g}_0 D\delta\left[t_1^2 + t_2^2 + \delta(t_1 + t_2) + \frac{2}{3}\delta^2 - 2\tau^2 \right]}_{\mathbf{g}\cdot\mathbf{g}_0\text{ cross terms}} \right] \right), \quad [1]$$

1090-7807/01 $35.00

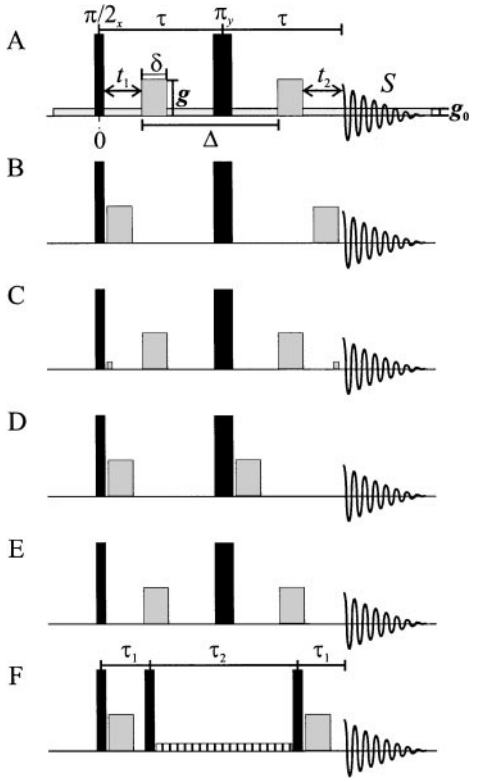

FIG. 1. Schematic diagram of the variations of the Hahn spin-echo-based PGSE pulse sequence (A–E) and the monopolar (F) and bipolar (G) stimulated-echo-based PGSE sequence. Radiation damping can occur during the periods in which the magnetization is not spatially encoded (i.e., during the periods t_1 and t_2 in A). The striped gradient pulse in F is a purge pulse for reducing the phase cycling requirements as well as preventing the onset of radiation damping during the τ_2 period (*43*).

where γ is the gyromagnetic ratio, Δ is the separation between the leading edges of the gradient pulses, and t_1 and t_2 are defined in Fig. 1A. Importantly, E is a function of the polarity of $\mathbf{g}$ due to the $\mathbf{g} \cdot \mathbf{g_0}$ term. When $g_0 \ll g$ Eq. [1] reduces to

$$E(g) = \exp(-\gamma^2 g^2 D\delta^2(\Delta - \delta/3)). \qquad [2]$$

In reality, the background gradient is a function of position in the sample (i.e., $\mathbf{g}_0 = \mathbf{g}_0(r, z)$, where (r, z) denotes the position of a volume element in cylindrical coordinates), and if the diffusing species moves between volume elements of different background gradient strength slowly (i.e., stays within a volume of constant g_0 during Δ), Eq. [1] becomes

$$E = \int_V E(g, g_0(r, z))\, dV. \qquad [3]$$

If the presence of g_0 is ignored and all gradient calibrations are performed using a sample of known diffusion coefficient and Eq. [2], the (apparent) value of g determined inherently contains the effects of g_0.

Modeling the Internal Macroscopic Gradients in an NMR Tube

To illustrate the background gradient problem due to magnetic susceptibility discontinuities, we have modeled the magnetic field in a standard NMR tube containing water (Fig. 2A). The components B_r and B_z of the static magnetic fields in a system with cylindrical symmetry can be calculated from the derivatives of the magnetic vector potential, A_φ (*27*),

$$B_r = -\frac{\partial A_\varphi}{\partial z} \quad \text{and} \quad B_z = \frac{\partial A_\varphi}{\partial r} + \frac{A_\varphi}{r}. \qquad [4]$$

A_φ depends on the electric current densities, J, and the magnetic permeability profile of the sample, μ_r. Since there is no static electric currents present, the magnetic vector potential satisfies the partial differential equation (*27, 28*)

$$\frac{\partial}{\partial r}\left(\frac{1}{\mu_r}\frac{\partial A_\varphi}{\partial r} + \frac{1}{r \cdot \mu_r} \cdot A_\varphi\right) + \frac{\partial}{\partial z}\left(\frac{1}{\mu_r}\frac{\partial A_\varphi}{\partial z}\right) = 0, \qquad [5]$$

with the boundary conditions

$$A_\varphi = 0.5 \cdot B_0 \cdot r \text{ at the external boundary of the sample} \qquad [6]$$

$$\frac{1}{\mu_r}\frac{\partial A_\varphi}{\partial n} \text{ is continuous at internal interfaces} \qquad [7]$$

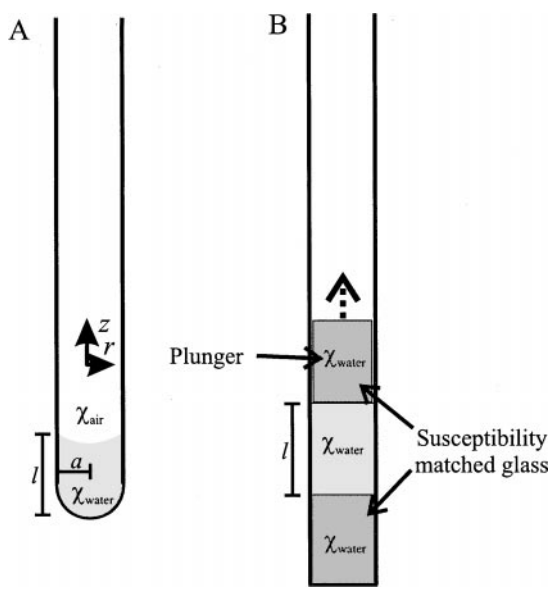

FIG. 2. Schematic diagram of (A) standard and (B) susceptibility matched NMR tubes. There is a large difference in magnetic susceptibility across the interface of the sample in the standard NMR tube due to the large difference in susceptibility between the air (χ_{air}) and the sample (i.e., water; χ_{water}). However, the glass in the susceptibility matched tube is approximately matched to the magnetic susceptibility of the sample.

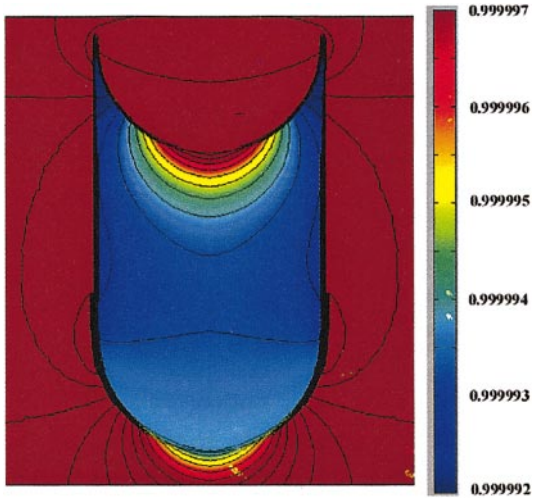

FIG. 3. Simulation of the background gradients in a standard NMR tube. Since the shape of the meniscus varies according to surface tension and the tube radius, we have arbitrarily modeled it as a half sphere. The simulations were performed using a radius (a) of 4.5 mm and a length (l) of 6.2 mm discretized into 10,000 mesh points and setting $\chi_{\text{air}} = 1$ and $\chi_{\text{water}} = 0.999991$. Each contour reflects a 0.5-ppm change in the field.

(i.e., $\frac{\partial A_\varphi}{\partial n}$ denotes the derivative of A_φ with respect to the normal vector).

Equations [5]–[7] were solved using the finite element method as contained in the MATLAB toolbox FEMLAB (*29*). The results are presented in Fig. 3. Since the errors in the numerical solution depend mainly on the used mesh size, it was decreased until no mesh size effects could be observed in the magnetic profiles.

Radiation Damping

Radiation damping results from the precessing spin magnetization generating an oscillating current in the receiver coil, which in turn generates an oscillating magnetic field, which rotates the magnetization back to its equilibrium position. Radiation damping can be characterized by a rate constant (*30*)

$$R_{\text{RD}} = \frac{1}{T_{\text{RD}}} = \kappa \eta Q, \qquad [8]$$

where η and Q are the filling and quality factors of the coil. The constant κ is defined by

$$\kappa = \frac{1}{2}\mu_0 \gamma M_z^{\text{eq}} = \frac{\mu_0 \gamma^3 \hbar^2 B_0 c_{\text{A}}}{8kT} \chi_{\text{water}}\ (\text{s}^{-1}),$$

where μ_0 is the permeability of free space, M_z^{eq} is the equilibrium magnetization, c_{A} is the number of protons (water protons in the present case) per unit volume, and χ_{water} is the magnetic susceptibility of water. Thus, the effects of radiation damping are much more serious in larger static fields and higher-Q NMR probes. Radiation damping is effectively inhibited when the net transverse magnetization is zero, such as when the magnetization is spatially encoded by a gradient pulse. For example, a gradient pulse applied along the long axis (which we take as being the z-direction) of a cylindrical sample immediately after a $\pi/2$ excitation pulse winds the magnetization into a helix along the z-axis with a pitch of $2\pi/(\gamma \delta g)(=1/q)$ (*31*). Hence, the attenuation of the net transverse magnetization signal for a sample of length l due to spatial encoding is

$$E_{\text{phase}}(g) = \frac{\int_{-l/2}^{l/2} e^{i\gamma \delta g z} dz}{l} = \text{sinc}\left(\frac{\gamma g \delta l}{2}\right). \qquad [9]$$

Hence, there is zero net transverse magnetization for complete rotations of the helix. Thus, in PGSE sequences radiation damping is most problematic in periods where the magnetization is not spatially encoded (i.e., during t_1 and t_2 in Fig. 1A).

EXPERIMENTAL

Experiments were performed at 298 K on Bruker DRX 300 and DMX 500 NMR spectrometers operating at ^{1}H resonance frequencies of 300 and 500 MHz, respectively. On both spectrometers, a 5-mm inverse (z-) gradient probe coupled with a BGAPA10 amplifier was used. The experiments on the effects of background gradients were performed using the proton signal from the residual ^1H_2O in ^2H_2O (Isotec, OH) in both a normal 5-mm NMR tube (Wilmad, NJ) and a 5-mm susceptibility matched tube (Shigemi, Tokyo; Fig. 2B). The experiments on the effects of radiation damping were performed using a sample consisting of 5 μL ethanol, 20 μL ^2H_2O, and 175 μL ^1H_2O in a 5-mm susceptibility matched tube.

The experimental parameters used for probing background gradient effects were $\tau = \Delta = 25$ ms and $\delta = 2$ ms (rectangular shaped) with sequence D in Fig. 1. For experiments involving radiation damping sequences, B–F were used with $\tau = \Delta = 70$ ms (except in sequence B where $\tau = 36.2$ ms, the minimum value of τ possible) and $\delta = 2$ ms (sine shaped). Sine-shaped gradient pulses were used to ensure that sequence B was unaffected by eddy current effects (*5*). In sequence F, a 0.005 T m^{-1} rectangular gradient pulse was used for the duration of τ_2 to both minimize the phase cycling requirements and prevent the initiation of radiation damping. The gradient strengths were calibrated using a small capillary of water (*32*) for the experiments at 300 and at 500 MHz, the residual ^1H_2O in ^2H_2O ($D = 1.90 \times 10^{-9}$ m^2 s^{-1} (*33*)).

The experiments were analyzed by regressing Eq. [2] onto the spin-echo attenuation data (integrals) using the Levenberg–Marquardt nonlinear least squares algorithm (*34*). The errors represent the 80% confidence limit from Monte Carlo simulations (*35*).

RESULTS AND DISCUSSION

Background Gradients

A series of ^{1}H PGSE NMR measurements of the residual water in ^2H_2O were performed using the same gradient settings (either positive or negative) and experimental conditions in a standard NMR tube and a susceptibility matched tube (see Fig. 2) with different sample volumes. Typically, the region of constant gradient is at most 1 cm long and thus, as it is important to keep the sample within the constant volume of the applied gradient (e.g., see Ref. (*36*)), we performed all of the experiments with relatively short samples (i.e., sample volumes $\leq$100 μl). A short sample also reduces convection and RF inhomogeneity artifacts. The results are summarized in Table 1. Although background gradients result in nonlinear attenuation plots when plotted in the usual semi-log fashion (see Eq. [1]) (*11*), the experimental data normally appear quite linear with the only signature of the background gradients being a slight initial concave up or down inflection of the attenuation curve at very small values of the applied gradient pulse.

As shown in Table 1, there is a significant difference (6%) in the observed diffusion coefficient depending on the polarity of the gradients for a standard NMR tube and this difference increases threefold as the sample volume is decreased from 100 to 50 μl. The agreement between the diffusion coefficient obtained using positive or negative polarity was much better when the susceptibility matched tube was used. However, when the susceptibility matched plunger was removed from the sample, the polarity dependence of the measured diffusion coefficients was even larger (43%) than that for the 50-μl sample in the standard tube and the nonlinearity of the attenuation plots was quite apparent (Fig. 4).

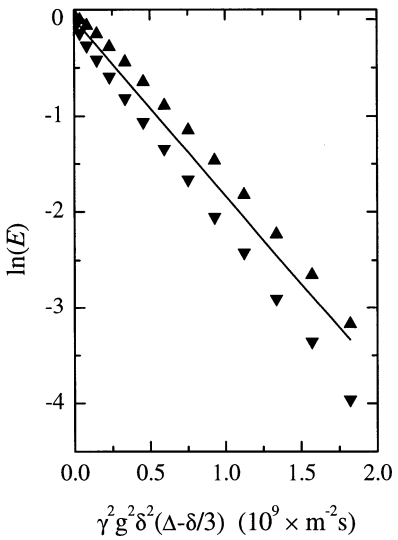

FIG. 4. PGSE NMR attenuation plot for the residual water in 50 μl of ^2H_2O in a susceptibility matched tube but without the plunger acquired using positive gradient polarity (▲) and negative gradient polarity (▼). The data were acquired at 300 MHz. Regression of Eq. [2] onto the average of the normalized positive and negative polarity data (solid line) gives a diffusion coefficient of $1.831 \pm 0.01 \times 10^{-9}$m^2 s^{-1}. Only the low gradient value data are shown to allow the background gradient-induced curvature to be clearly seen.

An obvious means of minimizing background gradients is simply to make the sample much longer, as is usually done in high-resolution NMR (NB compare the results for the 50- and 100-μl samples in the standard tube). However, the sample soon extends beyond the volume of constant gradient. Thus, this "solution" merely trades the background gradient problem for nonconstancy of the applied gradient (e.g., see Fig. 3 in (*7*)). An argument is often made that since the receptive volume of the RF coils is contained within the volume of constant gradient, thereby justifying the use of "long" samples; however, the validity of this argument is probe dependent. Some images acquired using a modified Hahn spin-echo sequence containing a read gradient of a susceptibility matched and a standard 1D NMR tube are given in Fig. 5. The applied gradient is clearly quite constant up to a sample length of 14.4 mm, since the image width increases linearly with sample length as shown in Fig. 6. However, for sample lengths above this there is some deviation, as shown by the loss of linear dependence for the 16.2-mm sample. Although the sample in the susceptibility matched tube has a very precise cylindrical shape, the images of samples longer than 11.9 mm do not have sharp cutoff frequencies (i.e., "vertical sides"; compare images C and D in Fig. 5). The loss of vertical sides is probably largely due to increasing RF inhomogeneity as the sample moves away from the RF coil center. As a consequence of the increasing RF inhomogeneity away from

TABLE 1

Apparent Diffusion Coefficient (D) of Residual Water in ^2H_2O at 298 K Determined from Regressing Eq. [2] onto the PGSE Attenuation Data Acquired for the Two Different Sample Tube/Gradient Setups Using Sequence D in Fig. 1

NMR tube measuring freq (MHz)	Sample volume (μl)	Gradient direction	D ($10^{-9} \times$ m^2 s^{-1})	D_{av} ($10^{-9} \times$ m^2 s^{-1})
Standard tube	100	Up	1.926 ± 0.009	1.872
300 MHz		Down	1.823 ± 0.016	
	50	Up	2.075 ± 0.025	1.919
		down	1.762 ± 0.024	
Susceptibility	50	Up	1.859 ± 0.008	1.822
matched		Down	1.784 ± 0.003	
300 MHz				
Susceptibility	50	Up	2.243 ± 0.059	1.907
matched – plunger		Down	1.570 ± 0.041	
300 MHz				
Susceptibility	50	Up	2.365 ± 0.055	1.933
matched – plunger		Down	1.501 ± 0.043	
500 MHz		Bipolar	1.902 ± 0.011	

Note. Also shown is the average value obtained using positive and negative gradient direction experiments, D_{av}. The value obtained using the 13 interval of Cotts *et al.* (*9*) (i.e., a bipolar gradient version of sequence Fig. 1F; see Fig. 4A in (*9*) but analyzed using Eq. [1] of (*37*)) is also given.

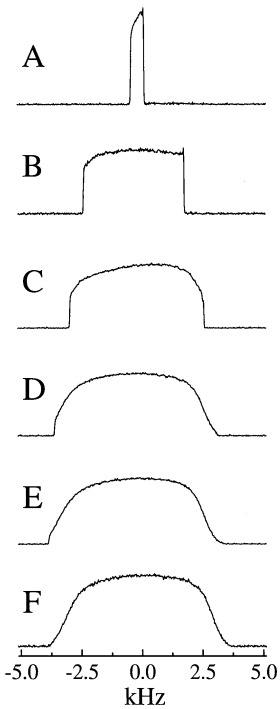

FIG. 5. ^{1}H images of the residual water along the long (i.e., *z*) axis of a susceptibility matched tube containing ^2H_2O to a height of (A) 1.3, (B) 9, (C) 11.9, (D) 14.4, and (E) 16.2 mm and (F) in a standard NMR tube to a height of 40.7 mm acquired at 500 MHz. The data were all acquired with the same read gradient (0.01 T m^{-1}). The uneven signal height is due to a combination of RF and applied gradient inhomogeneity and background gradients.

the sample center, the image of the sample in the standard NMR tube, although 40.7 mm long, appears only very slightly longer in frequency space than the 16.2-mm-long sample in the susceptibility matched tube. Thus, although the RF inhomogeneity limits the effective sample volume, it is, at least in the present case, slightly larger than the volume of constant gradient.

When analyzing PGSE experiments it has been claimed that integrals are preferable to using peak heights from both signal-to-noise considerations and because non-Lorentzian lineshapes are commonly observed (e.g., in biological samples (*21*)). We experimentally observed, as has been noted previously (*6*), that by restricting the frequency width when computing the integrals of a resonance in a series of PGSE spectra, the artifactual increase (or decrease) in *D* due to the presence of background gradients is greatly reduced. Hence, the effects of the background gradients are more evident in the "wings" of the resonance, whereas the central part of the resonance (which can be quite narrow) reflects the more homogeneous central part of the sample volume. However, this procedure is not a comprehensive solution since the amount of signal to be excluded is not clearly defined and it cannot be applied in the case of overlapping resonances.

Apart from minimizing background gradients by using susceptibility matched tubes, bipolar PGSE sequences (*9, 14, 37*) can be used to efficiently circumvent their effects (see Table 1). However, the underlying assumption is that a diffusing molecule experiences a constant background gradient throughout the sequence (*9*) and this assumption can fail, especially with large Δ values (*14*). If bipolar pulses are unavailable and assuming that the background gradients are small and that the exchange between volume elements is slow, the effects can be reduced by averaging the normalized PGSE attenuation data from two identical experiments, but performed with opposite gradient polarity (see Table 1 and Fig. 4), as can be seen by taking the power series expansion of Eq. [1] (*38*). Slice selection has also been suggested as a means of obtaining signals from limited sample volume (*39–41*); however, its inclusion can reduce the signal-to-noise unless care is taken to refocus the magnetization after the slice selection.

Radiation Damping

Radiation damping, especially at higher field strengths, can cause strong resonances to effectively "relax" with a time constant of 100 ms (or less), which is of similar order to the length of a PGSE sequence. The sample used in these experiments contained a very small ethanol concentration in (a large concentration of) water. Thus, only the water resonance was subject to the effects of radiation damping.

We examined some variations of the Hahn spin-echo-based PGSE sequence and the STE-based PGSE sequence (Fig. 1): (i) Hahn echo with diffusion gradients immediately after the $\pi/2$ pulse and immediately before acquisition (sequence B), (ii) Hahn echo with defocusing gradients immediately after the $\pi/2$ and before acquisition (sequence C), (iii) Hahn echo with defocusing gradients immediately after the $\pi/2$ and π pulses (i.e., $\Delta = \tau$) (sequence D), (iv) Hahn echo with gradients symmetrically placed around the π pulse with $\Delta = \tau$ (sequence E),

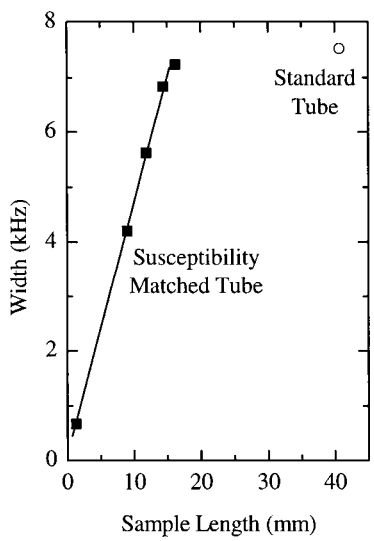

FIG. 6. A plot of the image width versus sample length for the images of the two tubes given in Fig. 5.

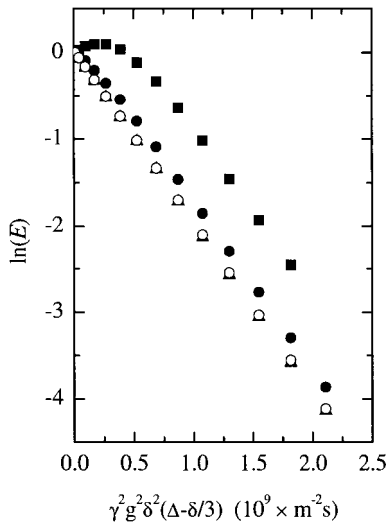

FIG. 7. Plots of the PGSE attenuation curves for the sequences (B, ▲; D, ■; E, ●; and F, ○) given in Fig. 1 acquired at 300 MHz. The data are normalized to the first positive value of g (=0.037 T m^{-1}) in each case. Note the rise and fall of the attenuation curve for sequence D due to the competition between radiation damping and diffusive attenuation.

(v) an STE-based sequence with the periods in which the magnetization is transverse kept short (i.e., the τ_1 periods) (sequence F). The attenuation plots of the H_2O resonance obtained using the various sequences are presented in Fig. 7 and the diffusion coefficients obtained for both the H_2O and the ethanol are summarized in Table 2.

An obvious solution to the radiation damping problem might seem to be to use a pulse angle much smaller than $\pi/2$ in the Hahn-based sequence; however, this approach fails since the π pulse then inverts almost all of the magnetization, thereby providing highly suitable conditions for initiating radiation damping. A better approach is to spatially encode the magnetization throughout the entire sequence (sequence B), although some delay is required after the second gradient pulse to allow eddy current dissipation. Fortunately, a delay of 100 μs was sufficient for the probe used in the present work, thereby allowing sequence B to be closely approximated. A related modification was then tried in which very small amplitude gradient pulses, such that the water magnetization should be completely dephased (see Eq. [9]), were applied immediately after the $\pi/2$ pulse and immediately before acquisition (i.e., sequence C). However, this approach failed due to the combination of the dipolar and radiation damping fields, causing the magnetization to recover in the form of a "superradiant pulse" after a delay after the gradient pulse (*26*) which depends on the area of the gradient pulse according to (*42*),

$$M(t) = (M_0 \cos\theta_0)\ \mathrm{sech}[(t - t_0')/T_{\mathrm{RD}}'], \qquad [10]$$

where

$$T_{\mathrm{RD}}' = T_{\mathrm{RD}}/\cos\theta_0 \qquad [11]$$

and

$$t' = -(T_{\mathrm{RD}}')\ln\left(\tan\frac{\tan^{-1}[\tan\theta_0 E_{\mathrm{phase}}(g)]}{2}\right).$$

In Eq. [11] M_0 represents equilibrium magnetization and θ_0 is the flip angle. Thus, in sequence C the gradients were too small to prevent the superradiant pulse from occurring before the diffusion gradients were applied and similarly to prevent a superradiant pulse from occurring during acquisition. The recovery of the magnetization is probably further complicated by the effect of background gradients since their magnitude would have been at least as large as the small applied gradient pulses.

The very different behavior of sequences D and E is due to the effects of radiation damping during the t_1 period. In sequence D, the t_1 period is negligibly short, and thus, for small amplitude gradient pulses, the signal is not much reduced by the beginning of the t_2 period in the sequence and, hence, the radiation damping effect occurs strongly during t_2 such that the transverse component of the signal is greatly reduced by the time acquisition begins. However, as the gradient strength is increased, the magnetization surviving through to t_2 is significantly reduced and thus radiation damping is less effective during t_2. Consequently, there is a competition between smaller signal loss due to radiation damping and greater signal attenuation due to diffusion as the gradient amplitude is increased. As the gradient strength continues to increase, the signal decrease due to radiation damping eventually becomes negligible and the diffusive attenuation dominates. This explains the strange increase and then decrease of the signal at small gradient values. In sequence E, radiation damping effectively relaxes much of the magnetization during t_1 such that the signal is too small to generate radiation damping problems during t_2.

TABLE 2
Apparent *D* Determined Using the Various PGSE Sequences (see Fig. 1)

Sequence	$D_{^1H_2O}$ ($10^{-9} \times m^2\,s^{-1}$)	D_{Ethanol} ($10^{-9} \times m^2\,s^{-1}$)	Remarks
B	2.01 ± 0.02	1.05 ± 0.01	Good fit
C	—	—	Failed
D	1.71 ± 0.06	1.03 ± 0.09	First six points removed
E	1.79 ± 0.03	1.06 ± 0.01	First three points removed
F	1.97 ± 0.00	1.08 ± 0.01	First point removed

Note. In the experiments, 15 different gradient values were used. In all cases (at least) the first point (i.e., $g = 0$) was removed. The data were acquired at 300 MHz.

Implications for Gradient Calibration and Diffusion Measurements

Background gradients are an insidious problem in PGSE measurements and generally cannot be ignored, even for homogeneous liquid samples. Since macroscopic background gradients are normally not symmetrical about $g_0 = 0$, their presence can be assumed if the measured diffusion coefficient is sensitive to the polarity of the applied gradient or if there is curvature in the attenuation plot at low gradient values. Ideally, the background gradients should be minimized as far as possible by using susceptibility matched NMR tubes and by using the minimum values of τ possible to accommodate Δ and eddy current effects (i.e., similar to sequence B) to minimize the cross term in Eq. [1]. For small background gradients the results of two experiments with opposite polarity can be used, but for this approach to be valid, Δ should be kept reasonably small so that the condition of slow exchange between regions of different background gradients holds. Alternatively, and especially when background gradients are large, more sophisticated sequences (e.g., bipolar gradients) should be used. To maximize the accuracy of PGSE measurements all samples should have the same volume, geometry, and magnetic susceptibility.

Radiation damping greatly complicates the performing of diffusion measurements of strong NMR resonances and can cause effects similar to those caused by background gradients. Apart from using a very small sample, the only two means by which accurate PGSE experiments can be conducted are: (1) by keeping all transverse magnetization spatially encoded during as much of the sequence as possible or (2) by allowing part of the magnetization to (reproducibly) decay before starting the diffusion part of the sequence.

ACKNOWLEDGMENTS

W.S.P. thanks the Swedish Council for International Cooperation in Research and Higher Education (STINT) for financial support. This work has been supported by grants from NFR and TFR.

REFERENCES

1. E. O. Stejskal and J. E. Tanner, Spin diffusion measurements: Spin echoes in the presence of a time-dependent field gradient, *J. Chem. Phys.* **42,** 288–292 (1965).
2. P. Stilbs, Fourier transform pulsed-gradient spin-echo studies of molecular diffusion, *Prog. NMR Spectrosc.* **19,** 1–45 (1987).
3. W. S. Price, NMR Gradient methods in the study of proteins, *in* "Annual Reports on the Progress in Chemistry Part C" (G. A. Webb, Ed.), pp. 3–53, Royal Society of Chemistry, London, 2000.
4. N. Hedin and I. Furó, Temperature imaging by ^{1}H NMR and suppression of convection in NMR probes, *J. Magn. Reson.* **131,** 126–130 (1998).
5. W. S. Price, K. Hayamizu, H. Ide, and Y. Arata, Strategies for diagnosing and alleviating artifactual attenuation associated with large gradient pulses in PGSE NMR diffusion measurements, *J. Magn. Reson.* **139,** 205–212 (1999).
6. I. Furó and H. Jóhannesson, Accurate anisotropic water-diffusion measurements in liquid crystals, *J. Magn. Reson. A* **119,** 15–21 (1996).
7. W. S. Price, Pulsed field gradient NMR as a tool for studying translational diffusion, Part II. Experimental aspects, *Concepts Magn. Reson.* **10,** 197–237 (1998).
8. S. Majumdar and J. C. Gore, Studies of diffusion in random fields produced by variations in susceptibility, *J. Magn. Reson.* **78,** 41–55 (1988).
9. R. M. Cotts, M. J. R. Hoch, T. Sun, and J. T. Markert, Pulsed field gradient stimulated echo methods for improved NMR diffusion measurements in heterogeneous systems, *J. Magn. Reson.* **83,** 252–266 (1989).
10. J. Zhong and J. C. Gore, Studies of restricted diffusion in heterogeneous media containing variations in susceptibility, *Magn. Reson. Med.* **19,** 276–284 (1991).
11. L. L. Latour, L. Li, and C. H. Sotak, Improved PFG stimulated-echo method for the measurement of diffusion in inhomogeneous fields, *J. Magn. Reson. B* **101,** 72–77 (1993).
12. M. D. Hürlimann, K. G. Helmer, L. L. Latour, and C. H. Sotak, Restricted diffusion in sedimentary rocks. Determination of surface-area-to-volume ratio and surface relaxivity, *J. Magn. Reson. A* **111,** 169–178 (1994).
13. G. H. Sørland, D. Aksnes, and L. Gjerdåker, A pulsed field gradient spin-echo method for diffusion measurements in the presence of internal gradients, *J. Magn. Reson.* **137,** 397–401 (1999).
14. J. G. Seland, G. H. Sørland, K. Zick, and B. Hafskjold, Diffusion measurements at long observation times in the presence of spatially variable internal magnetic field gradients, *J. Magn. Reson.* **146,** 14–19 (2000).
15. P. T. Callaghan, Susceptibility-limited resolution in nuclear magnetic resonance microscopy, *J. Magn. Reson.* **87,** 304–318 (1990).
16. S. Posse and W. P. Aue, Susceptibility artifacts in spin-echo and gradient-echo imaging, *J. Magn. Reson.* **88,** 473–492 (1990).
17. P. T. Callaghan, Susceptibility & diffusion effects in NMR microscopy, *in* "Encyclopedia of Nuclear Magnetic Resonance" (D. M. Grant and R. K. Harris, Eds.), pp. 4665–4671, Wiley, New York, 1996.
18. J. A. Glasel and K. H. Lee, On the interpretation of water nuclear magnetic resonance relaxation times in heterogeneous systems, *J. Am. Chem. Soc.* **96,** 970–978 (1974).
19. P. Gillis and S. H. Koenig, Transverse relaxation of solvent protons induced by magnetized spheres: Application to ferritin, erythrocytes, and magnetite, *Magn. Reson. Med.* **5,** 323–345 (1987).
20. D. T. Edmonds and M. R. Wormald, Theory of resonance in magnetically inhomogeneous specimens and some useful calculations, *J. Magn. Reson.* **77,** 223–232 (1988).
21. P. W. Kuchel and B. T. Bulliman, Perturbation of homogeneous magnetic fields by isolated single and confocal spheroids. Implications for NMR spectroscopy of cells, *NMR Biomed.* **2,** 151–160 (1989).
22. R. Bowtell and P. Robyr, Structural investigations with the dipolar demagnetizing field in solution NMR, *Phys. Rev. Lett.* **76,** 4971–4974 (1996).
23. J. Jeener, Dynamical effects of the dipolar field inhomogeneities in high-resolution NMR: Spectral clustering and instabilities, *Phys. Rev. Lett.* **82,** 1772–1775 (1999).
24. E. D. Minot, P. T. Callaghan, and N. Kaplan, Multiple echoes, multiple quantum coherence, and the dipolar field: Demonstrating the significance of higher order terms in the equilibrium density matrix, *J. Magn. Reson.* **140,** 200–205 (1999).
25. I. Ardelean and R. Kimmich, Demagnetizing field effects on the Hahn echo, *Chem. Phys. Lett.* **320,** 81–86 (2000).
26. Y.-Y. Lin, N. Lisitza, S. Ahn, and W. S. Warren, Resurrection of crushed magnetization and chaotic dynamics in solution NMR spectroscopy, *Science* **290,** 118–121 (2000).
27. J. D. Jackson, "Classical Electrodynamics," Wiley, New York, 1998.

28. G. Arfken, "Mathematical Methods for Physicists," Academic Press, New York, 1995.

29. FEMLAB, COMSOL, Inc., Burlington, MA, 1998.

30. J.-H. Chen, B. Cutting, and G. Bodenhausen, Measurement of radiation damping rate constants in nuclear magnetic resonance by inversion recovery and automated compensation of selective pulses, *J. Chem. Phys*. **112,** 6511–6514 (2000).

31. G. Deville, M. Bernier, and J. M. Delrieux, NMR multiple echoes observed in solid ^{3}He, *Phys. Rev. B* **19,** 5666–5688 (1979).

32. W. S. Price, H. Ide, and Y. Arata, Self-diffusion of supercooled water to 238 K using PGSE NMR diffusion measurements, *J. Phys. Chem. A* **103,** 448–450 (1999).

33. R. Mills, Self-diffusion in normal and heavy water in the range 1–45 degrees, *J. Phys. Chem.* **77,** 685–688 (1973).

34. W. H. Press, S. A. Teukolsky, W. T. Vetterling, and B. P. Flannery, "Numerical Recipes in C," Cambridge Univ. Press, Cambridge, 1992.

35. J. S. Alper and R. I. Gelp, Standard errors and confidence intervals in nonlinear regression: Comparison of Monte Carlo and parametric statistics, *J. Phys. Chem.* **94,** 4747–4751 (1990).

36. B. Håkansson, B. Jönsson, P. Linse, and O. Söderman, The influence of a nonconstant magnetic-field gradient on PFG NMR diffusion experiments. A Brownian-dynamics computer simulation study, *J. Magn. Reson.* **124,** 343–351 (1997).

37. D. Wu, A. Chen, and C. S. Johnson, Jr., An improved diffusion-ordered spectroscopy experiment incorporating bipolar-gradient pulses, *J. Magn. Reson. A* **115,** 260–264 (1995).

38. J. S. Murday and R. M. Cotts, Self-diffusion in molten lithium, *Z. Naturforsch.* **26a,** 85–93 (1971).

39. Ad. Bax and R. Freeman, Enhanced NMR resolution by restricting the effective sample volume, *J. Magn. Reson.* **37,** 177–181 (1980).

40. Y. Xia, Contrast in NMR imaging and microscopy, *Concepts Magn. Reson.* **8,** 205–225 (1996).

41. M. L. Tillett, L.-Y. Lian, and T. J. Norwood, Practical aspects of the measurement of the diffusion of proteins in aqueous solution, *J. Magn. Reson.* **133,** 379–384 (1998).

42. J.-H. Chen and X.-A. Mao, Experimental verification of the relation between the delay time and the tipping angle for a superradiant pulse, *J. Phys. D* **32,** 764–768 (1999).

43. W. S. Price, K. Hayamizu, and Y. Arata, Optimization of the water-PRESS pulse sequence and its integration into pulse sequences for studying biological molecules, *J. Magn. Reson.* **126,** 256–265 (1997).